FULL PAPER

Liver-Specific and Echogenic Hyaluronic Acid Nanoparticles Facilitating Liver Cancer Discrimination

Hyun Su Min, Sejin Son, Tae Woong Lee, Heebeom Koo, Hong Yeol Yoon, Jin Hee Na, Yongseok Choi, Jae Hyung Park, Jaeyoung Lee, Moon Hee Han, Rang-Woon Park, In-San Kim, Seo Young Jeong, Kyehan Rhee, Sun Hwa Kim, Ick Chan Kwon, and Kwangmeyung Kim**

With the increasing demand for instant real-time ultrasound (US) imaging of a specific organ, target-specific and long-circulating ultrasound contrast agents are of special interest. A new species of echogenic hyaluronic acid nanoparticles is presented as an ultralong-acting, liver-specific, US contrast agent that is distinct from conventional gas-filled microbubbles. Using an oil-in-water (O/W) emulsification method, bioinert and hydrophobic perfluoropentane (PFP) is encapsulated as an ultrasound gas precursor into hyaluronic acid nanoparticles (HANPs) using hydrophobic interactions. HANPs are formulated by self-assembly, with amphiphilic hyaluronic acid-5β-cholanic acid (HA-CA) conjugating in aqueous conditions. The resulting echogenic PFP-encapsulated HANPs (Echo-NPs) show solid nanostructures, differentiated from core-empty conventional microbubbles, and exhibiting outstanding physical properties as an ultrasound contrast agent. They are more stable and robust echogenic solid bodies with an in vivo favorable hydrodynamic size and because PFPs vaporize gradually, their expansion process is very slow in body conditions. After several systemic circulations, echo-NPs generated intense and ultralong echo signals for US imaging at the target site. The echogenic properties of Echo-NPs show a significantly increased half-life and echo persistence, compared with conventional microbubbles. The results clearly show that echo-NPs outperform conventional microbubbles in terms of both physical and echogenic in vitro and in vivo properties.

1. Introduction

Although ultrasound is one of the most important clinical imaging modalities, poor contrast sensitivity and extremely short time windows have been severe hurdles to clinicians, in particular, without the help of an ultrasound contrast agent (UCA).[1,2] A highly qualified UCA is a prerequisite for the widening spectrum of US technologies providing more informative images to clinicians.[3–7] However, the insurmountable conflicting problems of conventional UCAs, representatively microbubbles, comprised of an inert gas surrounded by stabilizing shells, such as polymers and lipids with a typical diameter of 1 to 8 μm,[8,9] have limited clinical applications of UCAs to intravascular imaging.[10] Conventional UCAs are quite unstable during systemic circulation, and their microdimensions are not suitable for intravenous (i.v.) administration.[11,12] Furthermore, due to their large particle sizes, microbubbles generally cannot diffuse out of the microvasculature into surrounding tissues after i.v. injection. In this context,

H. S. Min, Dr. S. Son, T. W. Lee, Dr. H. Koo, H. Y. Yoon, J. H. Na, S. H. Kim, Dr. I. C. Kwon, Dr. K. Kim
Center for Theragnosis
Biomedical Research Institute
Korea Institute of Science and Technology (KIST)
Hwarangno 14-gil 6, Seongbuk-gu, Seoul 136-791, South Korea
E-mail: Kim@kist.re.kr
H. S. Min, Prof. Y. Choi
School of Life Science and Biotechnology
Korea University
1 Anam-dong, Seongbuk-gu, Seoul 136-701, South Korea
T. W. Lee, Prof. S. Y. Jeong
Department of Life and Nanopharmaceutical Science
Kyung Hee University
1 Hoegi-dong, Dongdaemun-gu, Seoul 130-701, South Korea
H. Y. Yoon, Prof. J. H. Park
Department of Polymer Science and Engineering
Sungkyunkwan University
Suwon 440-746, South Korea
Prof. J. Lee, Prof. M. H. Han
Department of Radiology
Seoul National University Hospital
101 Daehangno, Jongno-gu, Seoul, 110-744, South Korea
Prof. R.-W. Park, Prof. I.-S. Kim
Department of Radiology
Seoul National University Hospital
101 Daehangno, Jongno-gu, Seoul, 110-744, South Korea
Prof. K. Rhee
Department of Mechanical Engineering
Myong Ji University
Yongin, South Korea
Prof. I. C. Kwon
KU-KIST School
Korea University
1 Anam-dong, Seongbuk-gu, Seoul 136-701, South Korea
E-mail: ikwon@kist.re.kr

DOI: 10.1002/adfm.201301131

a target-specific and highly qualified UCA, with both effective echogenic properties and in vivo behaviors, should guarantee the realization of true, real-time US imaging.[13–16]

Traditionally, there has been an insurmountable hurdle to the development of the ideal UCA: high echogenicity is offset by particle size reduction; the optimal particle size for effective extravasation of nanoparticles should be smaller than 750 nm, while particle size should be sub-micrometer sizes to obtain effective ultrasound contrast.[17–19] Therefore, the possibility of engineering nanosized UCA provides a clear advantage in the construction of an in vivo friendly UCA. The ideal UCA should meet the following criteria: 1) stability during bio-circulation and specific tissue accumulation, 2) echo signals persisting long enough to observe legions, 3) a size small enough to extravasate from vein to tissue. In this context, the newer approach of utilizing preformulated solid nanoparticles as templates to load liquid gas precursors provided several advantages in the construction of a long-acting UCA; greatly improved echogenic properties, and the precise tunability of particle size and polydispersity to go into systemic circulation.

Herein, we report new species of ultralong-acting, perfluoropentane (PFP) encapsulated, echogenic hyaluronic acid (HA) nanoparticles (Echo-NPs) for US (liver) imaging that demonstrate prominent physical properties distinct from conventional gas-filled microbubbles. Therefore, after echogenic HA nanoparticles were successfully formulated, their in vitro and in vivo echogenic and physical properties were thoroughly investigated, in preparation for their use in real in vivo US imaging applications.

2. Results and Discussion

2.1. Physical Properties of Echogenic HANPs

The new approach of utilizing pre-formulated solid hyaluronic acid nanoparticles (HANPs) to load liquid gas precursors may provide several advantages in the construction of a long-acting, nano-sized UCA. Interestingly, PFPs, as gas precursors, were confined in multiple hydrophobic inner cores inside the nanoparticles; therefore, the particle size could be rationally engineered to go into systemic circulation. Specifically, we prepared the echogenic HANPs using a simple o/w emulsification method. First, amphiphilic hyaluronic acid-5β-cholanic acid conjugates were self-assembled into HANPs in aqueous conditions, that is, induced by hydrophobic interactions between hydrophobic 5β-cholanic acid molecules conjugated to HA backbones[20] (**Figure 1**a). The average sizes of the resulting HANPs ranged from 350 to 450 nm, and their spherical shape was highly stable in aqueous solutions. In particular, the multiple hydrophobic 5β-cholanic acid inner cores were formed and located inside the outermost hydrophilic HA polymer shell layer,[21,22] which produced the unique nanostructures of HANPs. Second, an oil-phased PFP solution was mixed with the pre-formulated HANPs and emulsified to construct echogenic PFP-encapsulated HANPs (Echo-NPs) (Figure 1b), wherein PFP (1%, v/v), as an oil phase, was slowly added to the HANP solution (water phase) in an ice bath, followed by sonication process. The freshly produced Echo-NPs were very stable and stored for less than 1 h prior to use. As a control group, native HA polymer without hydrophobic CA moeities was used as a water phase to produce echogenic HA-coated PFP particles (Echo-HA). We assumed that native HA polymers without CA molecules could not form stable echogenic particles since HA polymers alone do not make self assembled nanoparticles.

Size distributions of the Echo-NPs were roughly gauged by optical microscopy combined with hydrodynamic size measurement. While gaseous Sonovue and Echo-HA showed fairly heterogeneous and large size distribution, with average diameters of 2889 ± 465 and 4160 ± 295 nm respectively, Echo-NPs demonstrated homogeneous and small size distribution, with an average diameter of 350 nm (**Figure 2**a,b). The authors assumed that Echo-NPs presented different physical and echogenic behaviors, compared to conventional gaseous UCAs, resulting from their unique and robust nanostructures. A comprehensive and comparative investigation gave us more insight and direct evidence regarding the differentiated and outstanding physical and echogenic properties of Echo-NPs and the advantageous factors they provided for in vivo biodistribution and specific organ targeting.[23,24] Considering that heterogeneous and large sized conventional microbubbles were major hurdles in developing an ideal UCA, this newer formulation strategy will provide an alternative, rational methodology.

More precise and informative TEM observations and insightful analyses of Echo-NPs nanostructures were performed to predict a gas forming mechanism and in vivo behaviors. In Figure 2c, the illuminated white spots are prominent in the inner core of Echo-NPs while there are no white spots in the bare HANPs without PFPs. Since we stained the polymeric parts of the HANPs negatively with uranyl acetate to enhance electron contrast, the illuminated white spots clearly indicate PFPs and the dim rings, located in the outermost shell area, indicate HA polymeric parts (Figure 2c, red arrows), respectively. On the contrary, in the simple mixture of HA and liquid PFP (Echo-HA), particle formation was not perfect, since whiter and larger white Echo-HA particles with submicron sizes and small polymeric HA particles without PFP existed together. Taking all these considerations into account, the extremely hydrophobic PFP liquid was absorbed into the HANPs hydrophobic CA multiple cores formulated by the o/w emulsion method. Furthermore, Echo-NPs showed higher negative-charged surface (ζ potential = –34.5 ± 3.8 mV), indicating that the negatively charged HANPs were highly distributed on the particle surface.

2.2. Temperature-Dependent Behaviors of Echo-NPs

Size variations of Echo-NPs were measured by dynamic light scattering (DLS) at each temperatures from 10 to 70 °C to predict their gas release and in vivo biodistribution behaviors. The size variations of Echo-NPs were evaluated as temperature was increased up to 70 °C; the hydrodynamic size of the Echo-NPs steadily increased from about 300 nm to 1 μm up to 60 °C. However, interestingly, a bimodal size distribution of 300 nm and 1.3 μm occurred at 70 °C, implying that extremely expanded Echo-NPs and flat Echo-NPs co-existed at this high temperature, since abruptly evaporated PFP gases expanded greatly or burst

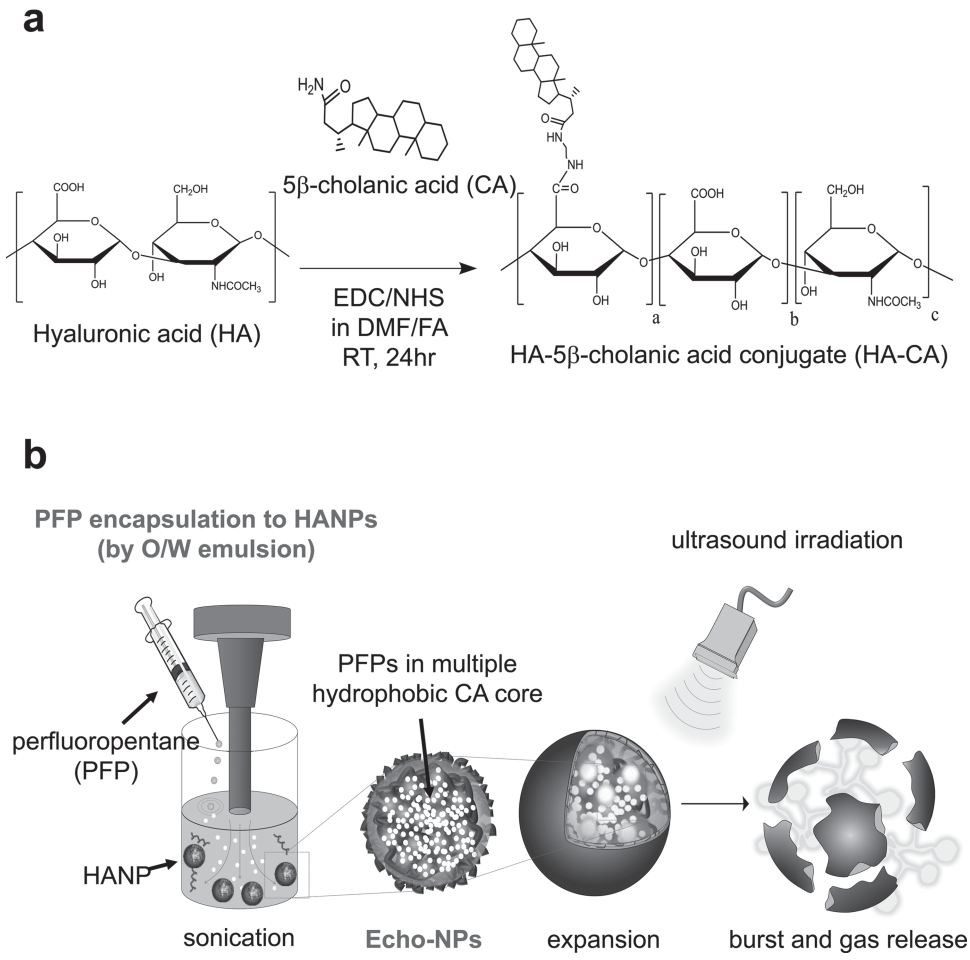

Figure 1. a) Synthetic scheme of amphiphilic HA-CA. b) Schematic representation of the new species of ultrasound contrast agent (Echogenic HA nanoparticles, Echo-NPs). Echo-NPs are formulated by the oil-in-water (O/W) emulsion method. Liver-specific and echogenic HANPs undergo expansion in body conditions (at 37 °C). As liquid PFPs evaporate gradually, there is partial PFP gas release from weak areas of the solid HANPs. Still, Echo-NPs support their shape to generate intense echo signals. Echo-NPs collapse or burst at temperatures above 60 °C or under US irradiation, since abrupt boiling of PFPs occurs.

the HANPs' scaffolds (**Figure 3**a). The explanation correlated well with the transmission electron microscopy (TEM) measurements (Figure 3b). When Echo-NPs were also monitored with increased temperature, it was clearly observed that partially evaporated PFP gases resulted in the expansion of the solid HANPs inner cores. However, after all, PFP gases were diffused out from relatively weak areas of the Echo-NPs, or burst the solid HANPs' scaffolds as temperature increase. In other words, robust HA-CA scaffolds can support the nanostructure of HANPs under the high pressure of evaporating PFP gas as they are expanding.

This aspect highlighted two advantages of the new species of Echo-NPs. First, the structural robustness of HANPs resulted in gas release retardation, which is the most critical reason for the ultralong-acting echo persistence. Second, the gas release retardation inside the Echo-NPs delayed also increase rate of the size of Echo-NPs, allowing repeated systemic circulation of Echo-NPs due to the in vivo friendly nanosize. The following sections extensively discuss these outstanding physical properties of Echo-NPs.

In order to evaluate the PFP vaporization retardation effect of robust Echo-NP scaffolds, size changes of Echo-NPs at different temperatures were measured by optical microscopy, and compared to those of Echo-HA and Sonovue (**Figure 4**a,b). While almost all Sonovue and Echo-HA disappeared within 20 min at 25 °C, Echo-NPs maintained their spherical nano-sized bodies, even under a high temperature of 60 °C, although the sizes increased. The bimodal size distribution was also observed at 60 °C. The increase of Echo-NP particle size was proportional to the increase of temperature, indicating that gas release was directly affected by external temperature. Therefore, since the temperature-dependent behaviors were not observed in Echo-HA and Sonovue, we concluded that the structural robustness of Echo-NPs was a critical factor in their improved colloidal stability, even though they did undergo a gradual expansion process. For practical application, it was most important that the size variations at body temperature (37 °C) benefitted Echo-NPs' in vivo behaviors. At 37 °C, a gradual increase of hydrodynamic size, ranging from 516 to 817 nm, was observed over a span of 20 min. Even though the size of the Echo-NPs reached 820 nm after 20 min, the rate of size increase was reasonable, and allowed enough time to perform in vivo imaging after

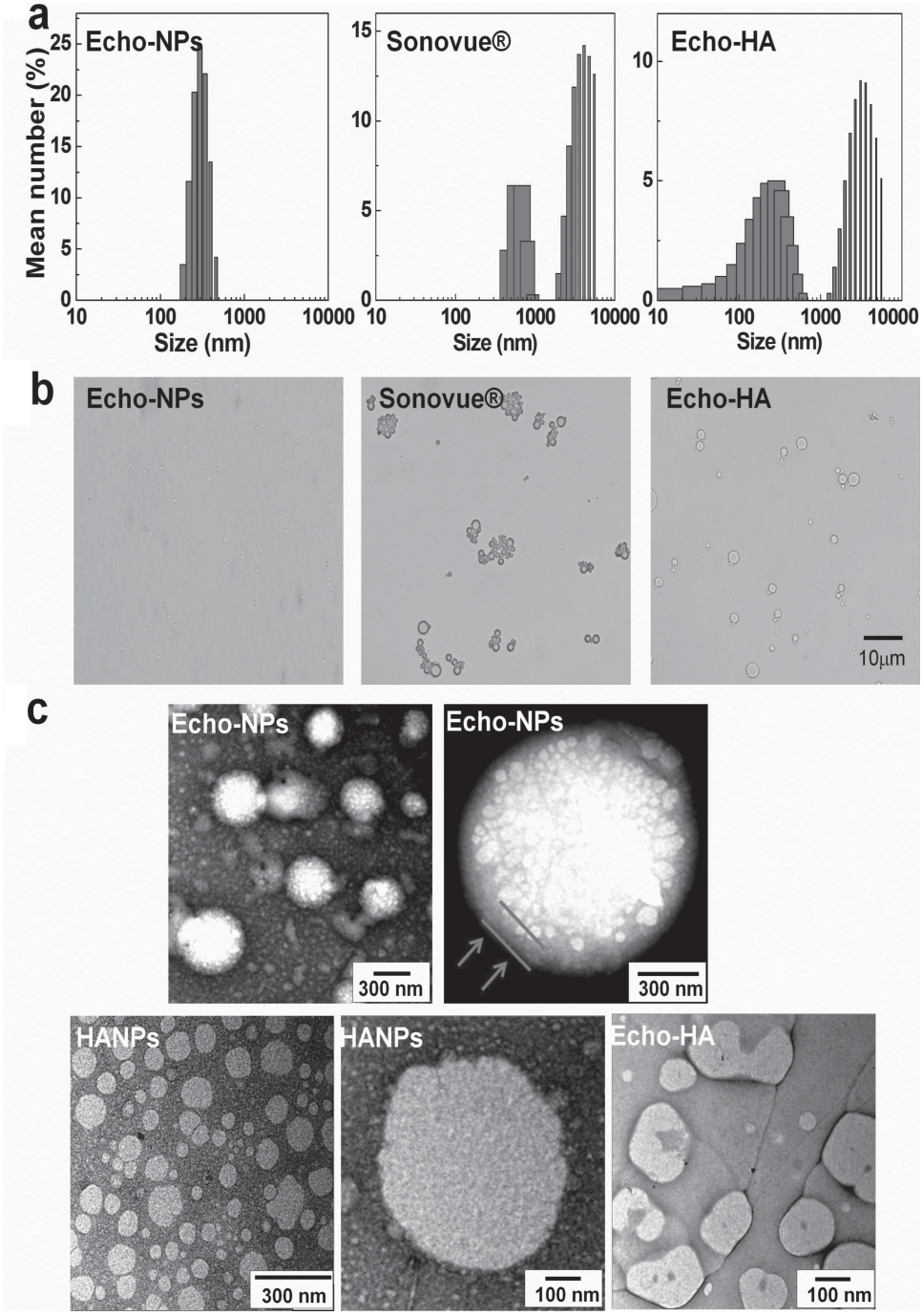

Figure 2. Characterization of Echo-NPs compared to those of Echo-HA and Sonovue. a) Physical properties in terms of hydrodynamic size and zeta potential, b) optical microscopy observation of monodispersed and small-sized Echo-HANPs in PBS at room temperature in contrast to extremely heterogeneous and large-sized Sonovue and Echo-HA. c) More precise observation of the inner structure and PFP localization inside Echo-NPs contrasted to those of bare HANPs without PFP and HA and PFP simple mixtures (Echo-HA). The prominent illuminated white spots were observed in the inner core of Echo-NPs, while there were no white spots in the bare HANPs, strongly implying that PFP localizes in the hydrophobic cholanic acid (CA) inner core inside HA shell layers (red arrows).

systemic circulation. Considering that the Echo-NPs reached the liver tissue within 30 s after i.v. injection (refer to in vivo US liver imaging data), the size of the Echo-NPs would still be ≈500 nm small enough to extravasate from liver vein to tissue.

2.3. In Vitro Echogenic Properties of Echo-NPs

To monitor the echogenic properties of Echo-NPs, agar-gel phantom test was done at the body temperature of 37 °C. When

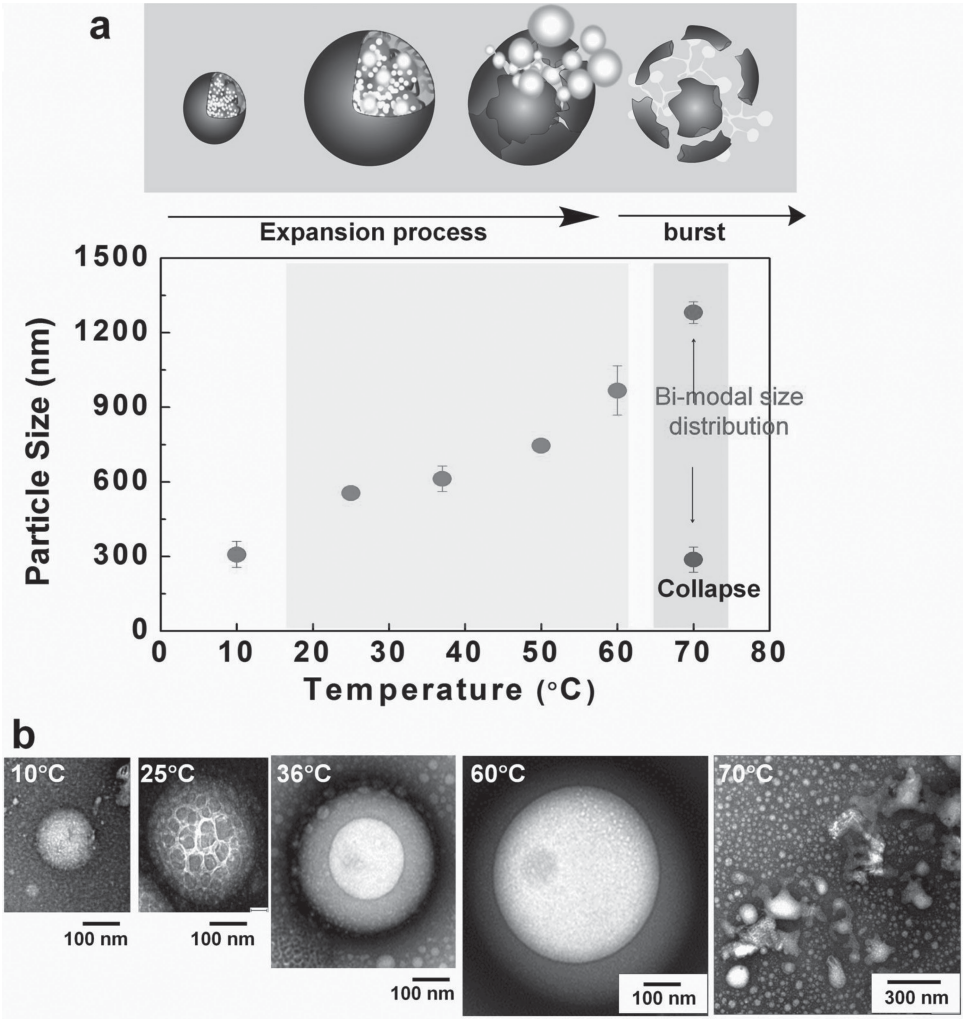

Figure 3. Temperature-induced PFP gas generating behaviors. a) Hydrodynamic size changes of Echo-NPs over temperature. At lower temperatures (25 °C), the particle size increases slightly, while the hydrodynamic sizes of Echo-NPs largely increase (37 °C). Further note the bimodal size distribution at higher temperatures (60 °C). b) Monitoring of the temperature-dependent gas generating process by TEM measurement. Expanded Echo-NPs were clearly observed as PFP evaporated gradually; finally, they are diffused out from relatively weak areas of Echo-NPs or Echo-NPs burst at the high temperature of 70 °C. c) Time-dependent (1 min and 20 min) size variations are investigated by optical microscopy at different temperatures. Most Sonovue and Echo-HA bubbles disappear after 20 min at 25 °C, which strongly indicates that they are quite unstable, even at room temperature. On the other hand, robust Echo-NPs were quite stable at 25 and 37 °C during 20 min, albeit they expanded abruptly at 60 °C.

the ratio of PFP to HANPs was increased from 0 to 5%, the generated US signals were proportionally increased also, but the echo intensity was almost saturated at 1.25% (**Figure 5**a,b). The echo persistence of Echo-NPs was also evaluated in agar-gel phantom with comparison to those of Echo-HA and Sonovue as control groups. As expected, Echo-NPs were persisted not fewer than 180 min (Figure 5c), and the half-life of echo signals is up to 135 min (Figure 5d,e). This persistence is note worthy that commercially available Sonovue and Echo-HA control groups were only persisted 12.5 min and 2.5 min respectively in the same US irradiation condition. The remarkably increased persistence can be rationalized by the direct comparison with that of Echo-HA. Above mentioned, since native HA polymer without hydrophobic CA moiety could not form self-assembled nanoparticles thereby Echo-HA particles with submicron sizes and small polymeric HA particles without PFP were co-existed, the resulted Echo-HA was quite unstable resulting in transient echo persistence. These transient echo properties were perfectly correlated with the TEM measurement and the temperature dependent size changes. Taken into account these results together, the structural robustness of Echo-NPs resulted in retarding gas release, in turn, leaded to the ultra long echo persistence as well as increase stability of Echo-NPs.

2.4. Hyaluronic Acid (HA)-Dependent Liver Targeting Efficiency

HA-dependent liver targeting ability was evaluated by a competitive inhibition assay using free HA treatment in Chang's liver (CL) cells. Chang's liver (CL) cells express a high level of the HA target receptor.[24–26] For visualization, Echo-NPs were labeled with fluorescent near-infrared (NIRF) dye. During

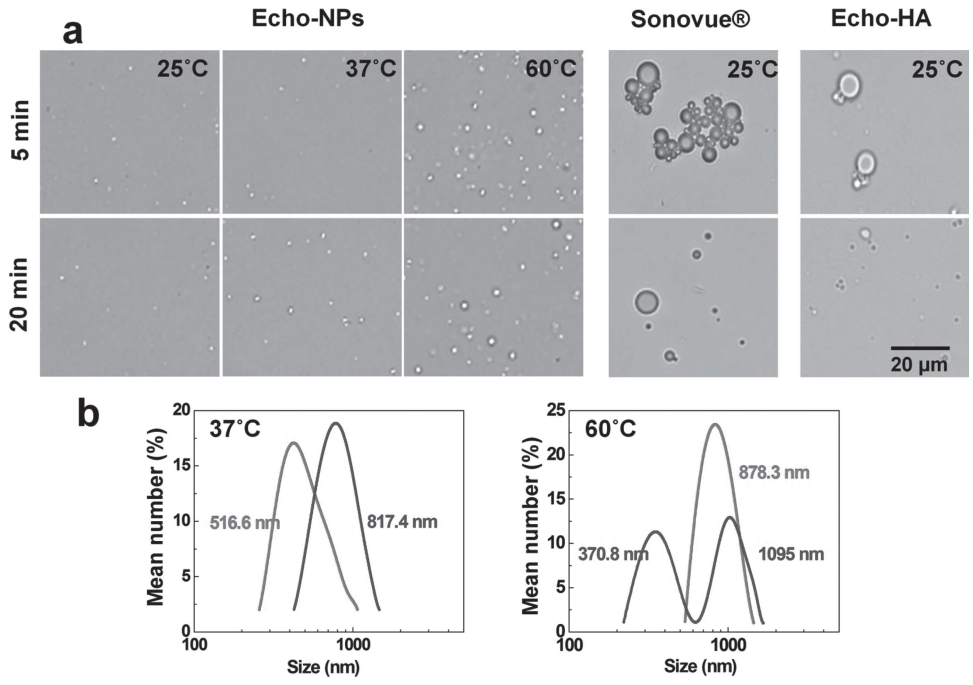

Figure 4. Size changes of Echo-NPs at different temperatures (at 25 °C and 60 °C) during 20 min were visualized by optical microscopy, and quantified by dynamic light scattering (DLS) measurement compared to those of Echo-HA and Sonovue. Almost Sonovue and Echo-HA bubbles disappear after 20 min at 25 °C, Echo-NPs maintained their spherical nanosized bodies, even under a high temperature of 60 °C, although the sizes increased.

pre-incubation with excess amounts of native HA, cellular uptake and/or binding of Echo-NPs was significantly inhibited in CL cells (**Figure 6**a) when compared to that during pre-incubation without pretreatment with native HA. The presence of native HA in the medium resulted in a significant decrease of fluorescent signals, which demonstrated that native HA and the HA motif on the surface of Echo-NPs competed with the same receptors on the cells.

HA-mediated liver targetability was also confirmed in a mice model after i.v. injections of Echo-NPs (Figure 6b,c). When Echo-NP-injected mice were sacrificed after 3 h, an intense NIRF signal was observed in the liver indicating the preferential accumulation of Echo-NPs in the liver. On the other hand, the NIRF signal in the liver was significantly reduced when an excess amount of native HA was pre-injected for competitive binding to the various HA receptors existing in the liver tissue. This result clearly shows that the preferential accumulation of Echo-NPs in the liver is highly dependent on the HA motifs on the Echo-NP's surface.

2.5. In Vivo US Imaging of Liver in Normal Mice

To evaluate the diagnostic potential of the Echo-NPs as a long-acting, liver-specific ultrasound contrast agent in vivo, the study included US imaging of the liver in mice models. No animals suffered any injuries, including burns, edema, and death, during this experiment. The contrast image was detectable as an increased scattering signal following reference subtraction of the pre-injection image. Liver-specific imaging signals were detected in all livers using contrast-enhanced US after the administration of Echo-NPs. Sonovue and Echo-HA were also tested together as control groups to verify the superiority of Echo-NPs in terms of in vivo echo persistence. On average, the mean difference in the normalized echo intensity in the liver was 99.9% after the administration of Echo-NPs, 100% after the administration of Sonovue, and 55.2% after the administration of Echo-HA, respectively. However, after 5 min, the difference in the echo intensity was not fewer than 3.5 times higher in the Echo-NPs group than in the both control groups, and that intensity was sustained up to 150 min in the livers of the mice in the same imaging session.

The remarkably increased echo persistence in the liver can be explained by their in vivo friendly physical properties. As mentioned above, the high affinity of HA to the liver could be a primary determinant, and the hydrodynamic size of Echo-NPs after i.v. injection could be a main factor. After i.v. injection, Echo-NPs start to circulate the body, and are captured in the liver by the specific HA-liver interaction (refer to Figure 5); they can diffuse out from the liver portal vein to the surrounding liver tissue because of their favorable size. The initial US images of the liver strongly supported this hypothesis. Within 1 min after the i.v. injection of Echo-NPs, several prominent spots, indicating the liver portal vein, were scattered in the liver. However, the prominent spots dissipated and the contrast was evenly distributed to all liver tissue. More interestingly, in the case of Echo-NPs, the contrast consistently increased up to 10 min and sustained the echo signals for not fewer than 140 min. On the other hand, with Echo-HA and Sonovue, the echo signals transiently persisted and the half-life of the echo signals occurred within 2 to 3 min, as expected (**Figure 7**b,c).

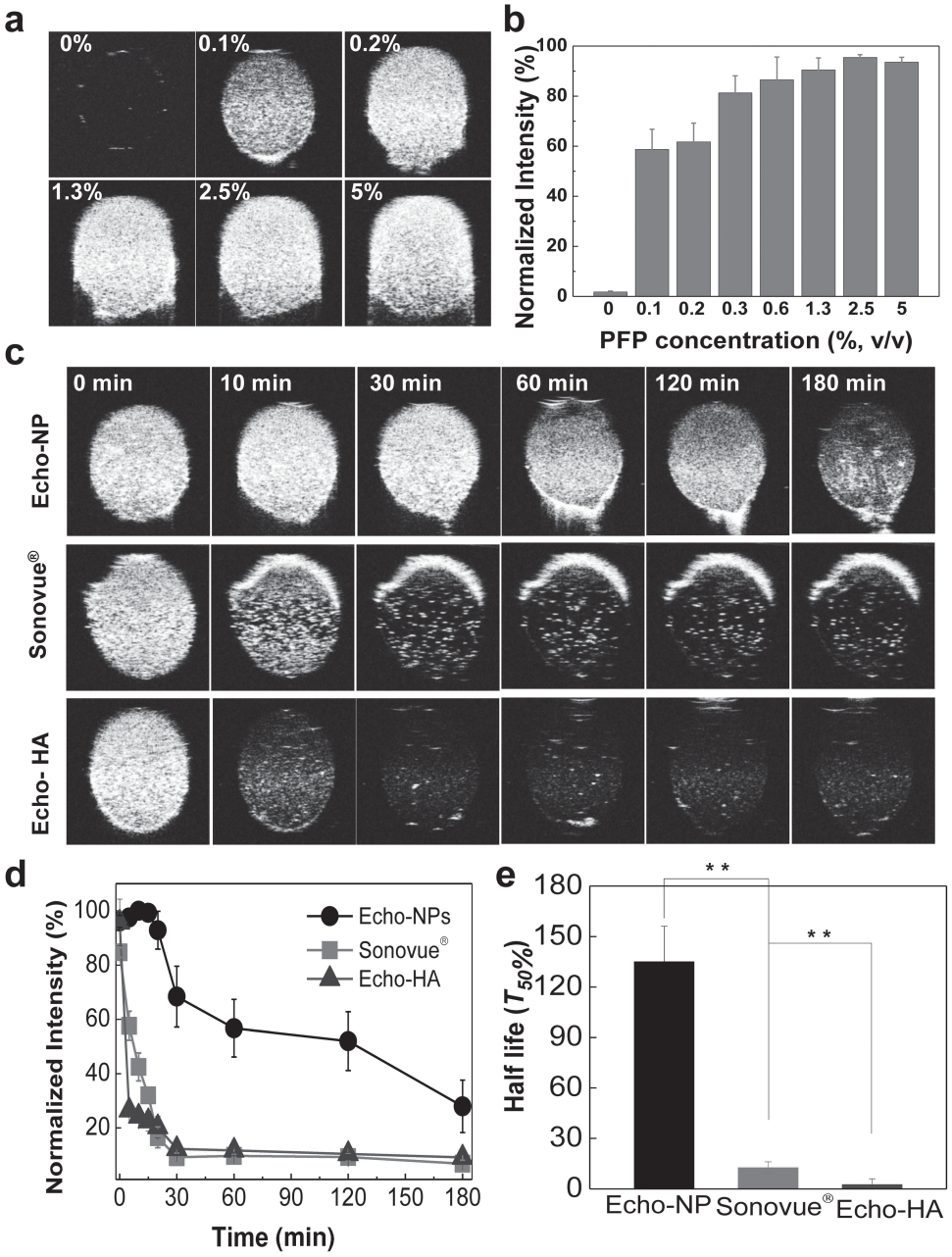

Figure 5. In vitro ultrasound images in various conditions. Hand-made agar gel phantom was used for in vitro US imaging and a frequency of 40 MHz was applied using a RMV 706 probe for imaging. US imaging intensities were normalized by subtracting the water intensity from the phantom signal. a) In vitro US images of Echo-NPs with the loading amounts of PFP in HA-CA solution. (0.08% to 5%, v/v). b) Normalized US intensities of Echo-NPs over PFP concentration. Increased US intensity with the PFP concentration and plateau intensity at 0.63%. c) Time-dependent echogenic behaviors of Echo-NPs, Sonovue, and Echo-HA at the same concentration (4 mg/mL) over time. d) Normalized US intensity of Echo-NPs, Echo-HA, and Sonovue with time. Echo-NPs showed significant long-term persistence compared to other control groups. e) Half-life of US intensity in agar gel phantom. Echo-NPs showed a 11 times longer half-life than that of Sonovue. The results represent the means ± SDs ($n = 4$); $^{**}P < 0.01$.

The robustness and increased stability of Echo-NPs in biodistribution sustained the echo intensity in the liver for more than 140 min. Echo-NPs reached the liver within 30 seconds after the i.v. injection; then, they circulated the whole body several times to refill into the liver portal vein. The relatively unstable Sonovue and Echo-HA, already comprehensively described in the formulation and characterization section, reached half life in only a few minutes (Figure 5c–e), making the US intensities in the liver dramatically transient: 8.6 min for Sonovue and 20 min for Echo-HA.

From these results, it is clear that the structural robustness of Echo-NPs resulted in their significantly increased half-life and liver accumulation. This robustness allowed Echo-NPs to circulate repeatedly through the liver, and enabled the liver to

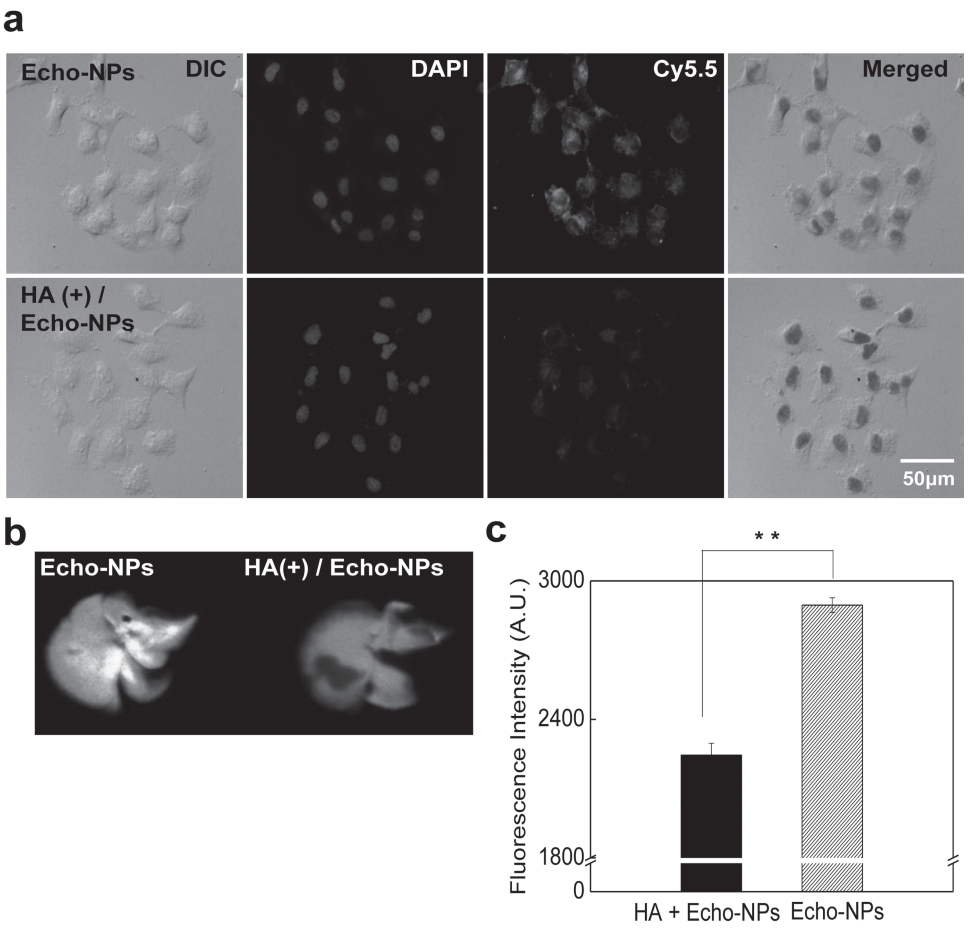

Figure 6. HA-dependent liver specificity of Echo-NPs. a) Normal liver cell binding and uptake efficiency of fluorescent cy5.5-Echo-NPs in CL-cells, with and without free HA pre-treatment. b) Ex vivo live imaging after i.v. injection of Echo-NPs in the mice model, with and without free HA pre-treatment. The results represent the means ± SDs ($n = 5$); $^{**}P < 0.01$.

capture the Echo-NPs mediated by HA-receptor interactions. Consequently, Echo-NPs gradually permeated liver tissues in a selective way and the liver retained them for an extended period.

2.6. Liver Cancer Discrimination

The earliest and most selective detection of cancer,[27] especially concerning metastatic cancer, is essential to surgical guidance and the monitoring of patient treatment, which is directly related to cancer mortality rates; the earlier these signatures can be established, the more effectively they can be treated.[28] However, it has been a major hurdle to detect lesions selectively from normal tissue, since the distinctions between normal tissues vs. metastatic cancer tissue are often subtle.[29] Above all, because all liver metastases begin with microscopic-sized, scattered small lesions,[30–33] sensitivity and specificity are the most desirable criteria for the development of a promising liver metastatic cancer imaging.

The exceptionally promising structural robustness and liver-specific echo persistence of Echo-NPs encouraged us to US image of liver cancer discrimination. We developed a liver tumor-bearing mice model using laparotomy and direct injection of HT-29 tumor cells into the liver. When the liver cancer had grown to approximately 50 mm^3, checked using the Vevo770 system, liver cancer imaging was performed. After the i.v. injection of Echo-NPs into the liver tumor models, the US intensity in the normal liver tissue was evaluated over time. As a result, ultrasound contrast was increased steadily in the normal liver tissue and maximized within 10 min and persisted in a span of 60 min (**Figure 8**a). This trend was almost correlated with in vivo US images in the normal liver, as precisely described in the former section. On the contrary, faint US signals in the liver cancer legion compared to the normal liver tissue were detected. Quantitatively, the ultrasound contrast between them was almost double (Figure 8b). Interestingly, the distinct ultrasound contrast was observed in the boundary between normal liver and cancer lesion. Those strongly imply that histological difference between normal liver and cancer resulted in an obvious distinction of Echo-NP's tissue permeability resulting in a significant US contrast discrimination normal liver from cancer lesion. This hypothesis is rationalized by histological analysis of cancer bearing liver tissue wherein a clear histological identification of liver cancer from normal liver was observed (Figure 8c). Since the liver cancer tissue is more compact than normal liver tissue, large sized Echo-NPs can not penetrate from normal liver to

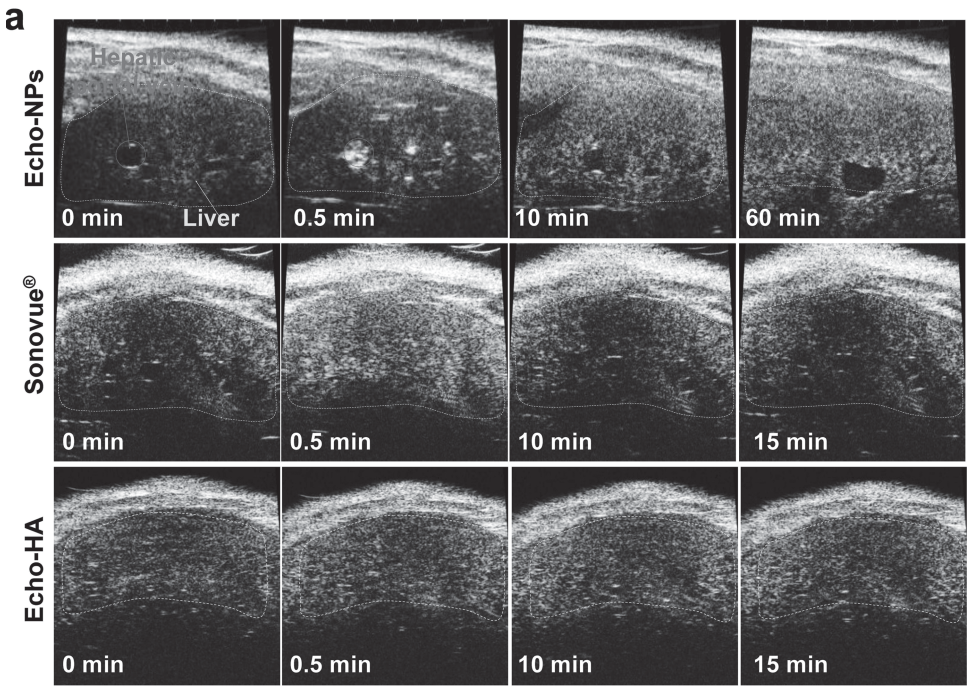

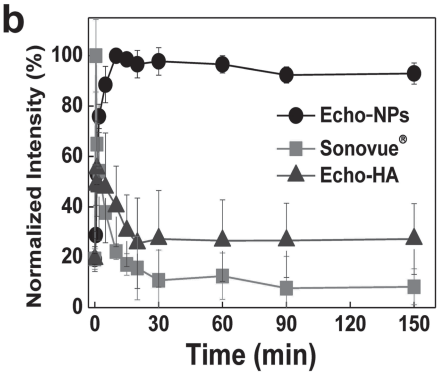

c

Types	Maximum Intensity	$T_{50\%}$ (min)
Echo-NPs	99.9±1.56	N.D.
Sonovue®	100±14.40	8.6±0.01
Echo-HA	55.2±18.9	20.7±0.15

Figure 7. In vivo US contrast enhanced images of mice liver over time. 300-μL samples were injected into the tail vein using a catheter syringe and 40 MHz of US was applied for imaging. a) US images of mice liver after tail vein injection of Echo-NPs, Sonovue, and Echo-HA respectively. b) Normalized US intensities in the liver over time. c) Comparative analysis of echogenic behaviors in the normal liver. Echo-NPs showed significantly intense echo signals comparable with Sonovue and long echo persistence ($T_{50\%}$) up to 150 min, while Sonovue and Echo-HA showed transient echo signals within 20 min.

liver cancer lesion. From this successful in vivo application of liver cancer discrimination, Echo-NPs were convinced of their medical value as a promising liver imaging agent.

3. Conclusions

This study developed a new species of echogenic HA nanoparticles as an ultralong-acting US contrast agent, which is distinct from conventional gas-filled microbubbles. Further, it proved the medical potential of Echo-NPs in a therapeutic mice model. Echo-NPs were quite stable, even during in vivo biocirculation; consequently, they showed exceptionally long echo persistence in targeted liver tissue. Through comprehensive and comparative investigations, the study confirmed that the structural robustness of the HANP scaffold was a decisive factor for their outstanding physical and echogenic properties. Therefore, we are convinced that Echo-NPs will provide a clinically useful medical US imaging agent, widening the therapeutic time window for clinicians in the field. Our new approach to construct gas-release echogenic nanoparticles can be expected to contribute to a more advanced design and a useful ultrasound contrast agent.

4. Experimental Section

Materials: Sodium hyaluronate (HA, Mw 250 KDa) was purchased from Lifecore Biomedical (Chaska, MN, USA), purified by washing with

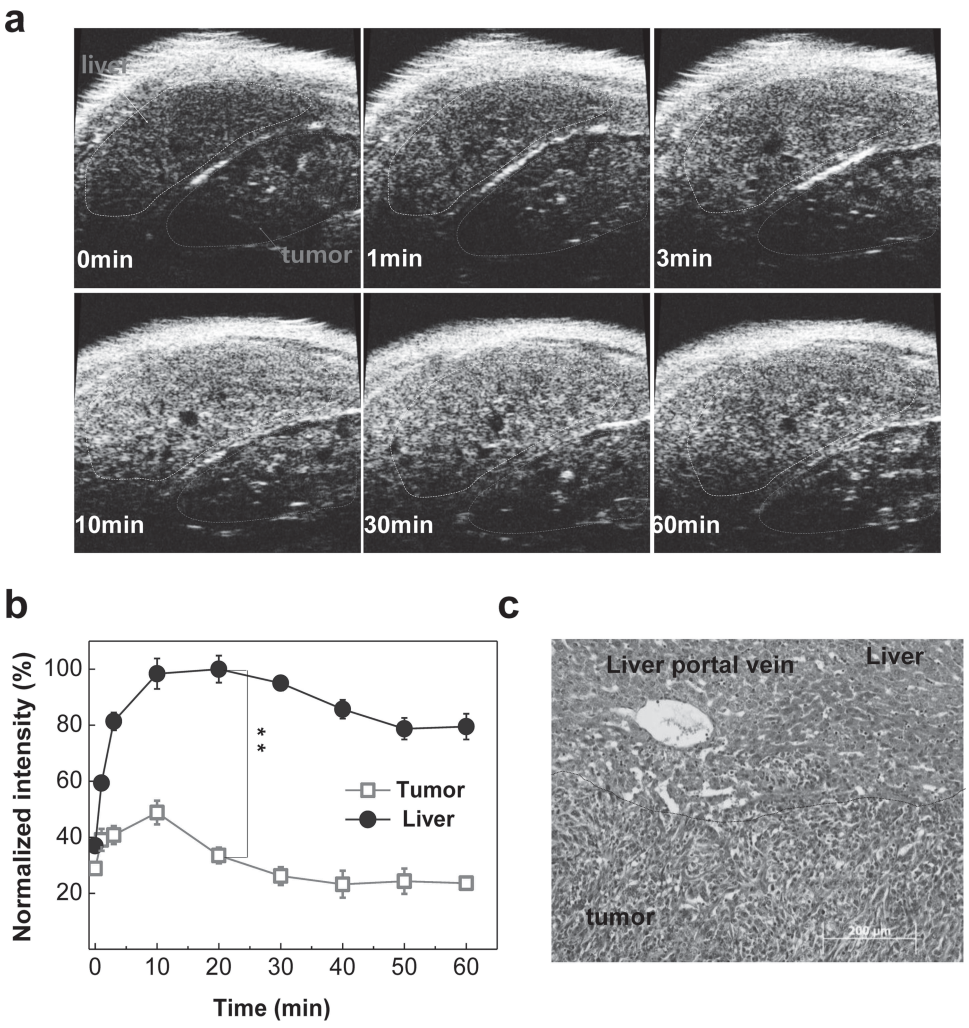

Figure 8. US images of liver in tumor-bearing mice over time. The liver tumor model was established using surgical implants of the HT-29 cell line; 40 MHz of US was applied for tumor imaging. For US imaging of the liver-tumor model, 300 μL of Echo-NPs (4.8 mg/kg) was i.v. injected via the tail vein. a) US contrast enhancement between the liver and the tumor site; yellow and red arrows indicate normal liver and tumor tissue, respectively. b) US imaging discriminating liver cancer from normal liver tissue. Normal liver shows 2.5 times higher enhanced contrast than does liver cancer. The results represent the means ± SDs ($n = 3$); $^{**}P < 0.01$. c) Histological analysis of the boundary between tumor and normal liver tissues by H&E staining.

deionized water and lyophilized after dialysis against distilled water prior to use. 5β-cholanic acid, *N*-hydroxysuccinimade (NHS), 1-ethyl-3-(3-dimethylaminopropyl)-carbodiimide hydrochloride (EDC), and dimethylsulfoxide (DMSO) were purchased from Sigma Chemical Co. (St. Louis, MO, USA). PFP (99%) was obtained from Apollo Scientific Ltd (Manchester, UK). Sonovue, commercial US imaging agent,was obtained from Bracco Diagnostics, Inc. (Milan, Italy).

Synthesis of HA-5-Cholanic Acid Conjugates (HA-CAs): Hydrophobically modified HA conjugates were synthesized using the chemical conjugation of 5β-cholanic acid to HA backbone.[19] Briefly, 5β-cholanic acid (2.8 mmol, 1 g) was aminated by hydrochloric acid (4.9 μmol, 180 μL) first, for amide linkage formation with the carboxyl group of HA in 5 mL of methanol. The products were lyophilized to obtain β-cholanic acid methyl ester. 300 mg of 5 β-cholanic acid methyl ester was dissolved in ethylenediamine (3 mL) and stirred for 6 h at 130 °C. The solution was purified with distilled water and lyophilized to obtain aminoethyl β-cholanoamide (EtCA). Second, HA (120 mg, 0.5 μmol) was dissolved in formamide (48 mL) and activated by EDC/NHS chemistry. After stirring the mixture vigorously for 15 min, EtCA (26.6 mg) in dimethylformamide was slowly added into the HA solution. The mixture was maintained for 24 h with stirring at room temperature. The resultant solution was purified using dialysis membrane (MWCO: 12–14 KDa, Spectra-Por, USA) against an excess amount of water/methanol (1:3 to 1:1, v/v) for 1 day and distilled water for 2 days, respectively. Purified HA-CA conjugates were lyophilized to obtain white powder.

Preparation of PFP-Encapsulated HANPs (Echo-NPs): Liver-specific echogenic nanoparticles were formulated by a simple o/w emulsification method with perfluoropentane (PFP) and HA solutions. First, amphiphilic HA-CA was dissolved in deionized water (4 mg/mL) and was filtered, using a 0.45 μm syringe filter (Whatman Int. Ltd., Springfield Mill, UK). Second, the HA-CA solution was transferred into an ice bath equipped with a probe type sonicator (ultrasonic processor 750-W, Cole-Parmer, IL, USA). Ten μl of PFP (1%, v/v), as an oil phase, was slowly added to the 1 mL of HA-CA solution (water phase) using a 34-gage syringe, while undergoing the sonication process (25% power, 2 min). As a control group, native HA polymers were also prepared using the same method as was used for Echo-NPs. After dissolving the HA polymer (250 KDa) in deionized water (4 mg/mL), 10 μL of PFP was

slowly dropped, then sonicated for 2 min, in the resulting Echo-HAs. Both echogenic particles were stored at 4 °C for less than 1 h prior to use.

Characterizations of PFP-HANPs: The size distribution and surface charges of Echo-NPs, Echo-HA, and Sonovue were measured by zeta-sizer (Malvern Zetasizer; Malvern Ins. Ltd., UK). Each sample was diluted in de-ionized water and size was measured at 25 °C. The temperature-dependent particle size distribution of Echo-NPs in deionized water was measured by increasing the temperature up to 70 °C. Also, the size distribution of each sample was directly visualized using optical microscope (BX51; Olympus Co. Ltd., Japan) equipped with 40× focal lens. The morphology of bare HANPs and Echo-NPs was directly determined using transition electron microscopy (TEM) (CM-200, Philips, CA). Freshly prepared HANPs and Echo-NPs, incubated for 20 min at 37 °C in deionized water, were dropped onto a 400-mesh copper grid, and stained with 5% (w/v) uranyl acetate solution after the water had been removed.

Cellular Uptake of Echo-NPs: To evaluate the cellular uptake of Echo-NPs to normal liver cells, an HA binding receptor inhibition study was conducted. CL-cells were seeded onto 35 mm gelatin-coated cover slips in 6-well plates (5×10^4/well) and washed twice with PBS. The CL-cells were treated with 8 mg/mL of diluted native HA polymer on the medium for 30 min to produce an inhibited condition of HA binding receptors on normal liver cells. To visualize fluorescent images of Echo-NPs on the cells, Cy 5.5 labeled Echo-NPs (10 μg/mL) were added, with and without receptor inhibited conditions. After 15 min post-incubation, the cells were washed with PBS for 5 min, fixed with fresh 4% paraformaldehyde, and mounted with Fluoromount-GTM (SouthernBiotech, Birmingham, AL). Microscopic images of the intracellular localization of the Echo-NPs were obtained using an IX81-ZDC focus drift compensating microscope (Olympus, Tokyo, Japan) with 675 nm excitation and 695 emission wavelength, respectively.

In Vitro US Imaging: In vitro US images were obtained using Vevo770 (High-Resolution Micro-Imaging System, Visualsonics, Toronto, Canada), equipped with a RMV 706 probe. In order to simulate body conditions for US imaging, the study used hand-made agar-gel phantom, made by embedding a 500 μL ependorf tube in the agar-gel (3%, w/v) and then removing the tube after the phantom gel had cooled. For in vitro experiments, 300 μL samples were administrated into agar-gel phantom and imaged with 40 MHz of ultrasound.

To evaluate the enhancement of US intensity via PFP contents, various ranges of PFP containing Echo-NPs (0.08–1.25%) were kept at 37 °C for 1 min before US images were obtained in agar-gel phantom. The US durability of Echo-NPs was compared to Echo-HA and Sonovue, respectively. The change of US intensity for each sample was measured up to 180 min, and the US intensity of the water control was subtracted from the sample intensity as the normalizing process.

In Vivo US iImaging of Normal Liver Tissue: All animal experiments with animals were conducted according to the relevant laws and institutional guidelines of the Korea Institute of Science and Technology (KIST) and institutional committees. Five and a half-week-old male BALB/c mice ($n = 3$ per each group, 25–30 g body weight) were used for in vivo US imaging. Before the US imaging, the mice were anesthetized using isofluorane gas and abdominal hair was removed with depilatory cream. Mice were positioned in an animal pad (Vevo770 maintained at 37 °C) and the liver was imaged using a RMV706 probe. After obtaining pre-injection liver images, 300 μL of Echo-NPs (48 mg/kg) were injected into the tail vein using a catheter syringe, and all the US images was recorded as a video file. The US images of the liver were obtained within 3 h and enhanced intensity was calculated by subtracting the ROI between the background of aqua-gel and normal liver tissue. To compare the durability of Echo-NPs to other samples, US images of the liver were also obtained after injections of Echo-HA (48 mg/kg) and Sonovue (60 mg/kg), using the same method.

US Imaging of Liver Cancer Discrimination: The liver cancer model was established using surgical implants of HT-29, a human colon-cancer cell line, into mice liver. HT-29 cells were cultured in RPMI cell culture media containing 10% FBS and penicillin G/streptomycin at 37 °C, CO_2 atmosphere. C3H/HeN ($n = 3$, 25–30 g) mice were anesthetized using intraperitoneal injections of ketamine (80 mg/kg)/xylazine (10 mg/kg) prior to laparotomy for direct injection of HT-29 cells (3×10^5) into the left lobe of the liver. When the liver cancer had grown to approximately 50 mm^3, checked using the Vevo770 system, liver cancer imaging was performed. Tumor bearing mice were anesthetized using isofluorane gas and positioned in animal pads for imaging. After finding the boundaries of the liver and cancer sites using Vevo770, pre-injection images was obtained. Then, 300 μL of Echo-NPs (4.8 mg/kg) was intravenously injected via catheter syringe. 40 MHz of ultrasound was applied for in vivo imaging over a 1-h period. To normalize the imaging intensity process, the ROI of the liver and cancer sites was calculated between the background of aqua-gel and the liver and cancer tissues.

Acknowledgements

H.S.M. and S.S. contributed equally to this work. This study was funded by the Fusion Technology Project (2010-50201) of MEST and grant No. RTI04-01-01 from the Regional Technology Innovation Program of the Ministry of Knowledge Economy (MKE), National R&D Program for Cancer Control of Ministry for Health and Welfare (1020260), and the Intramural Research Program (Theragnosis) of KIST.

Received: April 2, 2013
Published online: June 19, 2013

[1] V. R. Stewart, P. S. Sidhu, *Br. J. Radiol.* **2006**, *79*, 188.
[2] J. K. Willmann, N. van Bruggen, L. M. Dinkelborg, S. S. Gambhir, *Nat. Rev. Drug Discovery* **2008**, *7*, 591.
[3] H. S. Min, E. Kang, H. Koo, J. Lee, K. Kim, R.-W. Park, I.-S. Kim, Y. Choi, I. C. Kwon, M. Han, *Biomaterials* **2012**, *33*, 936.
[4] E. Kang, H. S. Min, J. Lee, M. H. Han, H. J. Ahn, I.-C. Yoon, K. Choi, K. Kim, K. Park, I. C. Kwon, *Angew. Chem. Int. Ed.* **2010**, *49*, 524.
[5] D. Vlaskou, O. Mykhaylyk, F. Krotz, N. Hellwig, R. Renner, U. Schillinger, B. Gleich, A. Heidsieck, G. Schmitz, K. Hensel, C. Plank, *Adv. Funct. Mater.* **2010**, *20*, 3881.
[6] M. A. Malvindi, A. Greco, F. Conversano, A. Figuerola, M. Corti, M. Bonora, A. Lascialfari, H. A. Doumari, M. Moscardini, R. Cingolani, G. Gigli, S. Casciaro, T. Pellegrino, A. Ragusa, *Adv. Funct. Mater.* **2011**, *21*, 2548.
[7] J. P. Frampton, Z. Fan, A. Simon, D. Chen, C. X. Deng, S. Takayama, *Adv. Funct. Mater.* **2013**, DOI: 10.1002/adfm.201203321.
[8] S. Hernot, A. L. Klibanov, *Adv. Drug Delivery Rev.* **2008**, *60*, 1153.
[9] V. Sanna, G. Pintus, P. Bandiera, R. Anedda, S. Punzoni, B. Sanna, V. Migaleddu, S. Uzzau, M. Sechi, *Mol. Pharmaceut.* **2011**, *8*, 748.
[10] F. Kiessling, J. Gaetjens, M. Palmowski, *Theranostics* **2011**, *1*, 127.
[11] J. A. Feshitan, C. C. Chen, J. J. Kwan, M. A. Borden, *J. Colloid Interface Sci.* **2009**, *329*, 316.
[12] H. P. Rim, K. H. Min, H. J. Lee, S. Y. Jeong, S. C. Lee, *Angew. Chem. Int. Ed.* **2011**, *50*, 8853.
[13] Y. Takei, A. Maruyama, A. Ferdous, Y. Nishimura, S. Kawano, K. Ikejima, S. Okumura, S. Asayama, M. Nogawa, M. Hashimoto, Y. Makino, M. Kinoshita, S. Watanabe, T. Akaike, J. J. Lemasters, N. Sato, *FASEB J.* **2004**, *18*, 699.
[14] B. Smedsrod, H. Pertoft, S. Eriksson, J. R. Fraser, T. C. Laurent, *Biochem. J.* **1984**, *223*, 617.
[15] B. Zhou, J. A. Weigel, A. Saxena, P. H. Weigel, *Mol. Biol. Cell* **2002**, *13*, 2853.
[16] T. Seternes, K. Sorensen, B. Smedsrod, *Proc. Natl. Acad. Sci. USA* **2002**, *99*, 7594.
[17] S. K. Hobbs, W. L. Monsky, F. Yuan, W. G. Roberts, L. Griffith, V. P. Torchilin, R. K. Jain, *Proc. Natl. Acad. Sci. USA* **1998**, *95*, 4607.
[18] R. B. Campbell, *Anti-Cancer Agents Med. Chem.* **2006**, *6*, 503.

[19] L. T. Quentin, S. Hervé, D. Marie-Hélène, *Nanotechnol. Rev.* **2013**, *2*, 125.
[20] K. Y. Choi, K. H. Min, J. H. Na, K. Choi, K. Kim, J. H. Park, I. C. Kwon, S. Y. Jeong, *J. Mater. Chem.* **2009**, *19*, 4102.
[21] K. Y. Choi, H. Y. Yoon, J. H. Kim, S. M. Bae, R. W. Park, Y. M. Kang, I. S. Kim, I. C. Kwon, K. Choi, S. Y. Jeong, K. Kim, J. H. Park, *ACS Nano* **2011**, *5*, 8591.
[22] S. Y. Han, H. S. Han, S. C. Lee, Y. M. Kang, I. S. Kim, J. H. Park, *J. Mater. Chem.* **2011**, *21*, 7996.
[23] Y. Malam, M. Loizidou, A. M. Seifalian, *Trends Pharmacol. Sci.* **2009**, *30*, 592.
[24] B. Haley, E. Frenkel, *Urol. Oncol.-Semin. Orig. Invest.* **2008**, *26*, 57.
[25] S. Urashima, M. Tsutsumi, K. Ozaki, M. Tsuchishima, K. Shimanaka, Y. Ueshima, S. Takase, *Alcohol.: Clin. Exp. Res.* **2000**, *24*, 34S.
[26] H. Lee, H. Mok, S. Lee, Y. K. Oh, T. G. Park, *J. Controlled Release* **2007**, *119*, 245.
[27] P. J. A. Robinson, *Br. J. Radiol.* **2000**, *73*, 234.
[28] K. Pantel, R. H. Brakenhoff, B. Brandt, *Nat. Rev. Cancer* **2008**, *8*, 329.
[29] A. Bajaj, O. R. Miranda, I. B. Kim, R. L. Phillips, D. J. Jerry, U. H. Bunz, V. M. Rotello, *Proc. Natl. Acad. Sci. USA* **2009**, *106*, 10912.
[30] I. C. Sun, D. K. Eun, J. H. Na, S. Lee, I. J. Kim, I. C. Youn, C. Y. Ko, H. S. Kim, D. Lim, K. Choi, P. B. Messersmith, T. G. Park, S. Y. Kim, I. C. Kwon, K. Kim, C. H. Ahn, *Chemistry* **2009**, *15*, 13341.
[31] T. H. Kuo, T. Kubota, M. Watanabe, T. Furukawa, T. Teramoto, K. Ishibiki, M. Kitajima, A. R. Moossa, S. Penman, R. M. Hoffman, *Proc. Natl. Acad. Sci. USA* **1995**, *92*, 12085.
[32] J. M. McLoughlin, E. H. Jensen, M. Malafa, *Cancer Control* **2006**, *13*, 32.
[33] N. B. Ackerman, W. M. Lien, E. S. Kondi, N. A. Silverman, *Surgery* **1969**, *66*, 1067.